MCB
Journals.ASM.org

Loss of Cadherin-Binding Proteins β-Catenin and Plakoglobin in the Heart Leads to Gap Junction Remodeling and Arrhythmogenesis

David Swope, Lan Cheng, Erhe Gao, Jifen Li, and Glenn L. Radice

Center for Translational Medicine, Department of Medicine, Thomas Jefferson University, Philadelphia, Pennsylvania, USA

Arrhythmic right ventricular cardiomyopathy (ARVC) is a hereditary heart muscle disease that causes sudden cardiac death (SCD) in young people. Almost half of ARVC patients have a mutation in genes encoding cell adhesion proteins of the desmosome, including plakoglobin (JUP). We previously reported that cardiac tissue-specific plakoglobin (PG) knockout (PG CKO) mice have no apparent conduction abnormality and survive longer than expected. Importantly, the PG homolog, β-catenin (CTNNB1), showed increased association with the gap junction protein connexin43 (Cx43) in PG CKO hearts. To determine whether β-catenin is required to maintain cardiac conduction in the absence of PG, we generated mice lacking both PG and β-catenin specifically in the heart (i.e., double knockout [DKO]). The DKO mice exhibited cardiomyopathy, fibrous tissue replacement, and conduction abnormalities resulting in SCD. Loss of the cadherin linker proteins resulted in dissolution of the intercalated disc (ICD) structure. Moreover, Cx43-containing gap junction plaques were reduced at the ICD, consistent with the arrhythmogenicity of the DKO hearts. Finally, ambulatory electrocardiogram monitoring captured the abrupt onset of spontaneous lethal ventricular arrhythmia in the DKO mice. In conclusion, these studies demonstrate that the N-cadherin-binding partners, PG and β-catenin, are indispensable for maintaining mechanoelectrical coupling in the heart.

Proper mechanical and electrical coupling of cardiomyocytes are crucial for normal propagation of the electrical impulse throughout the working myocardium (30, 39). Junctional proteins concentrated at the termini of cardiomyocytes are responsible for the integration of structural information and cell-cell communication. The end-to-end connection between cardiomyocytes called the intercalated disc (ICD) consists of three main junctional complexes: adherens junctions, desmosomes, and gap junctions. Desmosomes and adherens junctions act as mechanical cell-cell adhesion junctions maintaining the structural integrity of the myocardium. Adherens junctions consist of N-cadherin, the primary classical cadherin expressed in heart muscle. Extracellularly, N-cadherins of apposing cells interact, while intracellularly, catenins, including β-catenin or plakoglobin (PG) and α-catenin, link N-cadherins to the actin cytoskeleton, forming a cell "adhesion zipper" (43). Desmosomes also provide cell-cell adhesion but do so through intracellular connection to intermediate filaments (20). Along with its function in adherens junctions, PG is also a component of desmosomal complexes. The gap junction provides intercellular communication via small molecules and ions that pass through a channel generated by a family of proteins called connexins. Gap junctions allow for electrical coupling of cardiomyocytes, ensuring the coordinated muscle contraction required for proper heart function. There is a growing appreciation for the integrated nature of the junctional complexes at the ICD and for how aberrant cell-cell coupling mediated through these junctions can lead to cardiomyopathy and an increased risk of arrhythmias.

There is evidence supporting an essential function for PG in maintaining the structural integrity of the myocardium from both animal models and human disease. PG-null mice exhibit abnormal desmosome structure in the heart and skin that results in embryonic lethality (9, 38). The human *JUP* gene encoding PG was the first mutation linked to the heart muscle disorder known as arrhythmogenic right ventricular cardiomyopathy (ARVC [MIM107970]) (32). Patients with ARVC exhibit progressive loss of cardiomyocytes that are replaced by fibrofatty tissue and show a propensity for sustained ventricular tachycardia and sudden cardiac death (SCD) (7, 14, 15, 40, 42). ARVC is considered a disease of the desmosome, since almost half of the patients carry a mutation in one of the five genes encoding desmosomal proteins expressed in the heart. Moreover, the importance of PG has recently been highlighted because patients suffering from ARVC, regardless of their desmosomal gene mutation, show diminished PG localization to the ICD (6). β-Catenin and PG, highly conserved members of the armadillo protein family, also function as transcriptional regulators via their ability to bind to members of the T-cell factor/lymphoid enhancer factor (TCF/LEF) family of transcription factors. There is evidence that PG can translocate to the nucleus resulting in activation of adipogenic genes, highlighting the potential dual function of these armadillo proteins in ARVC (18).

In contrast to PG, β-catenin is not required to maintain the mechanical junctions in the adult myocardium, presumably due to the upregulation of PG and its ability to substitute for β-catenin in the adherens junction of the β-catenin mutant mice (49). Conversely, although β-catenin can bind to the cytoplasmic domain of desmosomal cadherins in the absence of PG, it cannot form a functional link with desmoplakin, resulting in abnormal desmosome structure in PG-null keratinocytes (10). The ability of PG to bind to the cytoplasmic domain of both classical and desmosomal cadherins and to form a functional link with actin and intermediate filaments, respectively, provides a molecular explanation for the lack of a structural defect in the cardiac tissue-specific

Received 26 August 2011 **Returned for modification** 28 September 2011
Accepted 3 January 2012
Published ahead of print 17 January 2012
Address correspondence to Glenn Radice, glenn.radice@jefferson.edu.

doi:10.1128/MCB.06188-11

β-catenin knockout mice (49). Hence, the primary function of β-catenin in the adult myocardium is not as a structural protein but, rather, as a regulator of pathological growth via its ability to bind TCF/LEF transcription factors and activate genes involved in cardiac hypertrophy (12).

In the ventricular myocardium, gap junction channels are composed mainly of connexin43 (Cx43). Aberrant expression and distribution of Cx43, referred to as gap junction remodeling, plays an important role in arrhythmogenesis in many forms of heart disease, including hypertrophy, ischemia, and dilated cardiomyopathies (35). In support of this idea, depletion of Cx43-containing gap junction plaques results in the slowing of ventricular conduction velocity, leading to ventricular arrhythmias and SCD in mice (21). In ARVC, gap junction remodeling has been observed in the absence of structural heart disease (23), supporting a direct role for mutated junctional proteins in the dysregulation of Cx43 and subsequent arrhythmogenesis and SCD. However, the molecular mechanisms underlying electrical uncoupling and subsequent development of conduction abnormalities and arrhythmia remain poorly understood.

We have previously shown that cardiac tissue-restricted knockout (CKO) of PG recapitulated many features of ARVC, including myocyte loss, replacement fibrosis, inflammation, and dilated cardiomyopathy (31). However, despite gap junction remodeling, the PG CKO mice did not exhibit conduction abnormalities or susceptibility to induced arrhythmias and survived longer than expected. Interestingly, β-catenin was upregulated in the absence of PG, suggesting possible compensation by this closely related armadillo family member. Here, we report increased association between Cx43 and β-catenin in PG-deficient hearts, suggesting that β-catenin may enhance the function of the remaining gap junctions, thus protecting PG CKO mice from SCD. To further investigate this hypothesis, we generated double knockout (DKO) mice lacking PG and β-catenin in the adult heart. DKO mice exhibit cardiomyopathy, extensive gap junction remodeling, and SCD approximately 3 to 5 months after deletion of both genes. We conclude that while loss of either β-catenin (49) or PG (31) alone in the adult heart is not sufficient to induce conduction abnormalities in mice, deletion of both cytoplasmic linker proteins leads to disassembly of the cardiac ICD structure and lethal arrhythmias.

MATERIALS AND METHODS

Generation of PG/β-catenin DKO mice. Previously generated αMHC/MerCreMer; $PG^{flox/flox}$ (31) mice were mated with either β-$catenin^{flox/flox}$ or β-$catenin^{-/+}$ mice (Jackson Laboratories, Bar Harbor, ME) to produce αMHC/MerCreMer; $PG^{flox/flox}$; β-$catenin^{flox/flox}$ or αMHC/MerCreMer; $PG^{flox/flox}$; β-$catenin^{flox/-}$ animals. The $PG^{flox/flox}$ strain will be available at The Jackson Laboratory Repository (Jax stock number 017575). The mice were maintained on a mixed 129Sv-C57BL/6J genetic background. Mice were treated with tamoxifen (Tam) (Sigma) by intraperitoneal injection once a day for 5 consecutive days at a dosage of 80 mg per kg of body weight per mouse per day. All animal experiments were performed in accordance with the guidelines of the IACUC of Thomas Jefferson University.

Histological analysis. Hearts were isolated and fixed in 4% paraformaldehyde, dehydrated, and embedded in paraffin. Global heart architecture was determined from longitudinal 6-μm deparaffinized sections stained with hematoxylin and eosin (H&E). Fibrosis was detected with Masson's trichrome or acid fuchsin orange G stain. Cross-sectional cell area measurements were obtained at the level of the nucleus in cross-sectioned, H&E-stained myocytes. Surface areas were quantified using NIS-Elements D software (Nikon). A minimum of 100 myocytes from five different animals was quantified for each experimental group.

Western blotting. For Western blotting, hearts were homogenized in a modified radioimmunoprecipitation assay (RIPA) buffer (50 mM Tris-HCl [pH 7.5], 150 mM NaCl, 1 mM EDTA [pH 8.0], 1% NP-40, 0.5% Na deoxycholate, 0.1% sodium dodecyl sulfate [SDS]) containing protease inhibitors and phosphatase inhibitor cocktails I and II (Roche Diagnostics) and centrifuged at 12,000 × *g* for 15 min. Western blot analyses were performed with antibodies to N-cadherin (3B9; Invitrogen), β-catenin (71-2700; Zymed), αE-catenin (C2081; Sigma), αT-catenin (a kind gift from Frans van Roy, VIB-Ghent University, Ghent, Belgium), plakoglobin (15; BD Biosciences), desmoplakin (multiepitope cocktail; ARP), desmoglein-2 (a kind gift from My Mahoney, Thomas Jefferson University), plakophilin-2 (2a plus 2b; Fitzgerald), Cx43 (C6219; Sigma), and dephosphorylated Cx43 (13-8300; Zymed), which binds selectively to dephosphorylated S364/S365 (34). For normalization of signals, blotting was also performed with an anti-GAPDH (anti-glyceraldehyde-3-phosphate dehydrogenase) (6C5; RDI) monoclonal antibody, followed by incubation with an IRDye 680- or IRDye 800CW-conjugated secondary antibody (Li-Cor). Membranes were imaged with the Odyssey infrared imaging system (Li-Cor), and quantitative densitometric analysis was performed by applying Odyssey version 1.2 infrared imaging software.

Immunofluorescence analysis. Paraffin-embedded heart sections (6 μm) were mounted, dewaxed in xylene, rehydrated through an ethanol series, and then heated in 1× antigen unmasking solution (Vector Laboratories) in a microwave oven (350 W) for 10 min to unmask the epitope. Following blocking with 5% nonfat milk–phosphate-buffered saline (PBS) for 30 min, sections were incubated at 4°C for 16 h with primary antibodies diluted in 5% nonfat milk–PBS. The primary antibodies used are described above. After washing in PBS, sections were incubated with Alexa Fluor 488- or 555-conjugated goat anti-mouse or -rabbit antibody (Molecular Probes, Invitrogen) for 1 h at room temperature. After washing in PBS, sections were mounted using medium (Vectashield) containing DAPI (4′,6-diamidino-2-phenylindole). Slides were imaged using a Zeiss LSM 510 META confocal microscope system. Cardiomyocyte cell death was measured using an *in situ* cell death detection kit (Roche) and following the manufacturer's instructions. Representative images of the ventricle ($n \geq 10$ images and $n \geq 100$ nuclei per image) were counted for positive terminal deoxynucleotidyltransferase-mediated dUTP-biotin nick end labeling (TUNEL) staining in four different animals per group.

Adult mouse ventricular myocyte isolation and immunocytochemistry. Adult murine ventricular myocytes were isolated using the method previously described (33). Briefly, mice were heparinized (0.5 U/g intraperitoneally) and then anesthetized with 2,2,2-tribromoethanol (Avertin; 100 mg/kg intraperitoneally). Hearts were excised, mounted on a Langendorf apparatus, and perfused with Ca^{2+}-free Tyrode's solution for 6 min at 3.0 to 3.5 ml/min and a temperature of 36 to 37°C, followed by 12 to 15 min of perfusion with Ca^{2+}-free Tyrode's solution containing collagenase B and collagenase D (Roche Chemical Co.) plus protease (fraction XIV; Sigma Chemical Co.). When the hearts appeared pale and flaccid, they were removed from the Langendorf apparatus and the ventricles were dissected away and kept in Ca^{2+}-free Tyrode's solution with 1 mg/ml of bovine serum albumin (fraction V; Sigma Chemical Co.). The ventricles were teased into small pieces and then triturated gently with a Pasteur pipette to dissociate individual myocytes. Cells were then fixed in 4% paraformaldehyde for 20 min and subsequently suspended in PBS for immunostaining as described above. The immunofluorescence signal was analyzed by quantitative confocal microscopy using methods validated in previous studies (28, 41). This method is specifically designed to measure the amount of immunoreactive signal by quantifying the number of pixels concentrated in clusters showing high-intensity fluorescence. Twenty test areas were analyzed for Cx43 immunoreactivity for each genotype. Each test area was scanned within 21,389.06 μm^2 (146.25 μm by 146.25 μm) and digitized into a 1,024 by 1,024 matrix (1,048,576 pixels/test area) in

which 1 pixel equals 0.02 μm^2. The amount of immunoreactive signal in each test area was expressed as the percentage of total cell area by quantifying the total numbers of pixels in digitized images exceeding prospectively defined signal intensity thresholds divided by the total number of pixels occupied by tissue. The number and size (pixels) of individual clusters of high intensity signal within each test area were quantified with NIH Image 1.33u software.

TEM. Hearts were isolated and cannulated on a perfusion apparatus. Hearts were then pretreated in relaxation medium containing 100 mM KCl and fixed in 2% glutaraldehyde–1% paraformaldehyde in 0.08 M cacodylate buffer with 2 mM $CaCl_2$, pH 7.4, and processed for sectioning (70 nm) for transmission electron microscopy (TEM) (Jeol JEM1010). Measurements were conducted on a minimum of 10 fields per heart from three different animals per group.

M-mode, two-dimensional echocardiography. Transthoracic two-dimensional echocardiography was performed using the Vevo 770 high-resolution imaging system equipped with a 30-MHz probe (Visual Sonics) in anesthetized (2% inhaled isoflurane) wild-type (WT) ($n = 13$) and DKO mice ($n = 14$). The left ventricular (LV) wall thickness and dimension were measured from M-mode images from the parasternal short-axis view at the plane bisecting the papillary muscles. Values were obtained by averaging three consecutive cardiac cycles, and ventricular fraction shortening (FS) and ejection fraction (EF) were calculated. Doppler transthoracic echocardiography was conducted on the parasternal long-axis view for aortic valve (AoV) and pulmonary valve (PV) velocity measurements.

Electrophysiological studies. Adult mice were heparinized (0.5 U/g intraperitoneally) and then anesthetized with 2,2,2-tribromoethanol (Avertin; 100 mg/kg intraperitoneally). The hearts were quickly removed through a thoracotomy and rinsed in Tyrode's solution containing 130 mmol/liter NaCl, 24 mmol/liter $NaHCO_3$, 1.2 mmol/liter NaH_2PO_4, 1.0 mmol/liter $MgCl_2$, 5.6 mmol/liter glucose, 4.0 mmol/liter KCl, and 1.8 mmol/liter $CaCl_2$ and equilibrated with a 95% O_2, 5% CO_2 gas mixture. Hearts were then rapidly cannulated, perfused in a retrograde fashion via an aortic cannula with 37°C oxygenated Tyrode's solution (2 to 3 ml/min), and placed in a chamber. The solution in the chamber was used as a volume conductor for recording electrocardiograms (ECGs). ECGs were recorded with a Cyber Amp380 amplifier (Axon Instruments) and digitized at 10 kHz with a Digidata 1400A and AxoScope 10.2 after equilibration for 20 min. Bipolar pacing electrodes were placed on the epicardium of the ventricle. The ventricle was paced using pulses equivalent to 1.5× threshold amplitude with a 2-ms duration for 15 min. For ambulatory ECG monitoring, miniature telemetry transmitter devices were implanted as previously described (26). The leads were directed caudally and anchored into the ECG lead I position for long-term recording. Once the mice had fully recovered from the implantation procedure (48 to 72 h), their electrocardiograms were analyzed for any signs of spontaneous ventricular ectopy or atrioventricular conduction disturbances.

IP from whole heart tissue. Heart lysates were prepared as described for Western blotting. Samples (3 mg) of lysates were precleared using TrueBlot anti-rabbit or anti-mouse Ig coimmunoprecipitation (IP) beads (eBioscience) for 1 h at 4°C with rotation. After the beads were discarded, lysates were incubated for 60 min at 4°C with rotation with 10 μg of rabbit anti-Cx43 (C6219; Sigma) or mouse anti-N-cadherin (BD Biosciences). TrueBlot anti-rabbit or anti-mouse Ig IP beads (50 μl) were added to each reaction mixture, and the tubes were rotated further overnight at 4°C. Beads were washed four times for 5 min each time with 1 ml RIPA buffer on ice and once with 1 ml 1× PBS. Proteins were eluted from beads in 25 μl 2× NuPAGE sample buffer and subjected to SDS-polyacrylamide gel electrophoresis and Western blotting with the antibodies described above. Lysates subjected to incubation with IgG beads without antibody (−Ab) served as the negative control.

Statistics. Data are expressed as the mean ± the standard error of the mean (SEM). Comparisons between groups were performed with a two-tailed Student *t* test. Survival analysis was performed by the Kaplan-Meier method, and between-group differences in survival were tested by the log rank test. One-way analysis of variance (ANOVA) analysis was performed for comparison of Cx43 immunoreactivity between the four genotypes. A *P* value of <0.05 was considered statistically significant.

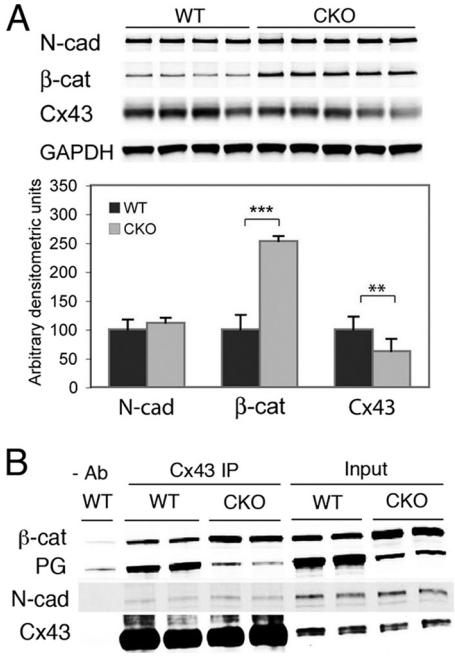

FIG 1 Increased β-catenin association with Cx43 in PG-deficient hearts. (A) Western analysis of WT and PG CKO heart lysates probed for N-cadherin (N-cad), β-catenin (β-cat), and Cx43. GAPDH (glyceraldehyde-3-phosphate dehydrogenase) served as a loading control. (B) Heart lysates were immunoprecipitated with anti-Cx43 antibody and subsequently immunoblotted for β-catenin, plakoglobin (PG), N-cadherin, and Cx43. No-antibody IP served as the negative control (−Ab). Note the increased association of β-catenin with Cx43 in PG CKO hearts. **, $P < 0.01$; ***, $P < 0.001$.

RESULTS

Increased β-catenin association with Cx43 in PG-deficient hearts. We previously reported that conditional knockout of PG in the heart (cardiac-specific PG knockout [PG CKO]) results in cardiac pathology and gap junction remodeling reminiscent of those in ARVC patients (31). However, despite decreased Cx43 expression at the ICD, PG CKO mice have no apparent conduction abnormalities and are not susceptible to arrhythmias, a prominent feature in ARVC patients. We hypothesize that the upregulation of β-catenin compensates for the loss of PG in the N-cadherin/catenin/Cx43 macromolecular complex, resulting in sufficient electrical coupling and thus protecting the PG CKO mice from arrhythmias. Adult αMHC/MerCreMer; $PG^{flox/flox}$ mice were administered tamoxifen (Tam) to induce deletion of the *PG* gene specifically in the myocardium as previously reported (31). No change in N-cadherin expression (Fig. 1A) or distribution at the ICD (31) was observed in the PG CKO hearts. Interestingly, β-catenin was significantly increased in the PG CKO hearts (Fig. 1A), suggesting that it may functionally compensate, at least partially, for loss of PG. To determine whether there was an increased interaction between β-catenin and the remaining Cx43, coimmunoprecipitation was performed with anti-Cx43 antibody and probed for β-catenin and PG, as well as N-cadherin. In wild-type (WT) hearts, both β-catenin and PG were found in a protein complex with Cx43 and N-cadherin (Fig. 1B). Importantly, when

PG was depleted, there was an increased association between Cx43 and β-catenin, suggesting that these two armadillo proteins compete for binding to the Cx43 multiprotein complex. Moreover, despite gap junction remodeling, the association between N-cadherin and Cx43 was not reduced in the absence of PG (Fig. 1A), suggesting a stable interaction between the remaining gap junctions and adherens junction components, which may explain the lack of arrhythmogenicity in the PG CKO mice.

Generation and characterization of PG/β-catenin DKO mice. To further investigate the role of β-catenin in the PG CKO mice, we generated αMHC/MerCreMer; $PG^{flox/flox}$; $\beta\text{-catenin}^{flox/flox}$ or αMHC/MerCreMer; $PG^{flox/flox}$; $\beta\text{-catenin}^{flox/-}$ mice. To inactivate both the PG and β-catenin genes specifically in the heart, PG/β-catenin double knockout (DKO) mice (6 to 8 weeks old) with and without the Cre transgene (47) were administered Tam for 5 consecutive days. Immunofluorescence analysis of heart sections displayed significant reduction of normally strong intercalated disc staining of both PG and β-catenin in DKO hearts 3 months after the administration of Tam (Fig. 2A to D). Moreover, Western analysis of heart lysates revealed a significant decrease in PG (−79%, $P < 0.001$) and β-catenin (−63%, $P < 0.001$) in DKO hearts compared to the levels in WT hearts (Fig. 2E). In contrast to mice with either single CKO, sudden death occurred in 100% of DKO mice (23/23) at between 3 and 5 months (105 days median survival), compared to 8.5% of PG CKO mice (9/105), 3.9% of β-catenin CKO mice (3/76), and 3.7% of WT controls (3/81) within 6 months after Tam administration (Fig. 2F).

Histological analysis demonstrated enlargement of both right and left ventricles in DKO mice compared to those of littermate controls 3 months after the administration of Tam (Fig. 3A and D). In the DKO hearts, fibroblasts were interspersed throughout the myocardium, accompanied by collagen deposition (Fig. 3E and F). Reminiscent of the PG CKO model (31), there was no increase in adipocytes in the DKO hearts. TUNEL analysis showed increased apoptotic cells in DKO hearts 3 months after Tam administration (2.27% for DKO mice versus 0.35% for WT mice, $P < 0.001$) (Fig. 3G to I). The DKO mice displayed a significant increase in heart weight/body weight ratios (7.67 mg ± 0.82 [DKO] versus 5.77 mg ± 0.67 [WT], $P < 0.001$) and cardiomyocyte cross-sectional area (12.45 μm ± 1.91 [DKO] versus 10.29 μm ± 1.69 [WT], $P < 0.001$), consistent with a hypertrophic response (Fig. 3J and K). The DKO mice did not exhibit signs of heart failure, such as liver or lung congestion (data not shown). Collectively, these data demonstrate a more severe cardiac pathology in the DKO than in either single-CKO mouse model (31, 49), which resulted in sudden death in 100% of the DKO mice.

Disassembly of mechanical junctions in PG/β-catenin DKO mice. To determine the consequences of deleting these two linker proteins on the expression of other adherens junctional and desmosomal components, we performed immunofluorescence and immunoblot assays on DKO hearts 3 months after Tam administration. Representative images of the ventricular myocardium illustrate the significant decrease in adherens junctional proteins N-cadherin, αE-catenin, and αT-catenin in DKO hearts (Fig. 4A to F). In addition to the loss of expression at the ICD evident by immunofluorescence, Western analysis revealed a considerable decrease in total N-cadherin protein levels (−89%, $P < 0.001$) in DKO hearts. Moreover, αE-catenin and αT-catenin were also significantly reduced in DKO hearts, −79%, $P < 0.001$, and −83%, $P < 0.001$, respectively (Fig. 4G). Desmosomal proteins were also

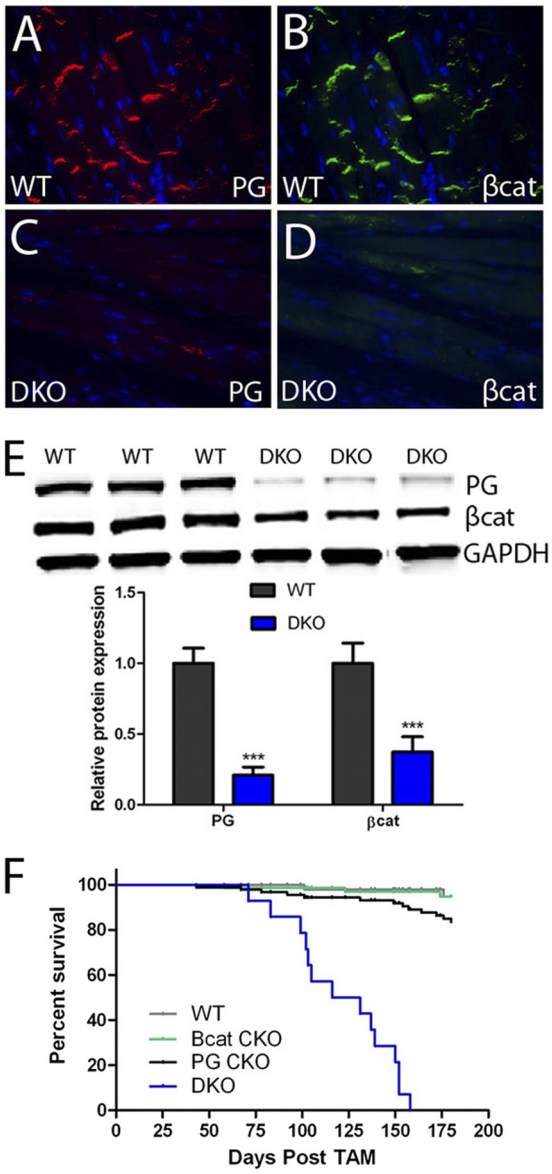

FIG 2 Sudden death in PG/β-catenin DKO mice. (A to D) Heart sections from $PG^{flox/flox}/\beta\text{-catenin}^{flox/flox}$; Cre^{-} (WT) (A and B) and $PG^{flox/flox}/\beta\text{-catenin}^{flox/flox}$; Cre^{+} (DKO) (C and D) mice were immunostained for plakoglobin (PG) (A and C) and β-catenin (βcat) (B and D) 3 months after Tam administration. (E) Heart lysates from WT ($n = 8$) and DKO ($n = 10$) mice were immunoblotted for PG and β-catenin. (F) Kaplan-Meier survival curve shows completely penetrant sudden-death phenotype in the DKO mice (23/23; median survival, 105 days), compared to the survival of PG CKO mice (9/105), β-catenin CKO mice (3/76), and WT controls (3/81) within 6 months after Tam administration. ***, $P < 0.001$.

affected in the DKO hearts (Fig. 5). Immunofluorescence analysis of the ventricular myocardium demonstrated loss of desmoplakin (Fig. 5A and D), plakophilin-2 (Fig. 5B and E), and desmoglein-2 (Fig. 5C and F) from the ICD in DKO hearts. Furthermore, immunoblot assays showed reductions in total protein levels for desmoplakin (−76%, $P < 0.01$), plakophilin-2 (−81%, $P < 0.001$), and desmoglein-2 (−45%, $P < 0.01$) in DKO hearts (Fig. 5G). Taken together, these data indicate that loss of PG and β-catenin lead to disruption of adherens junctions and desmosomes at the

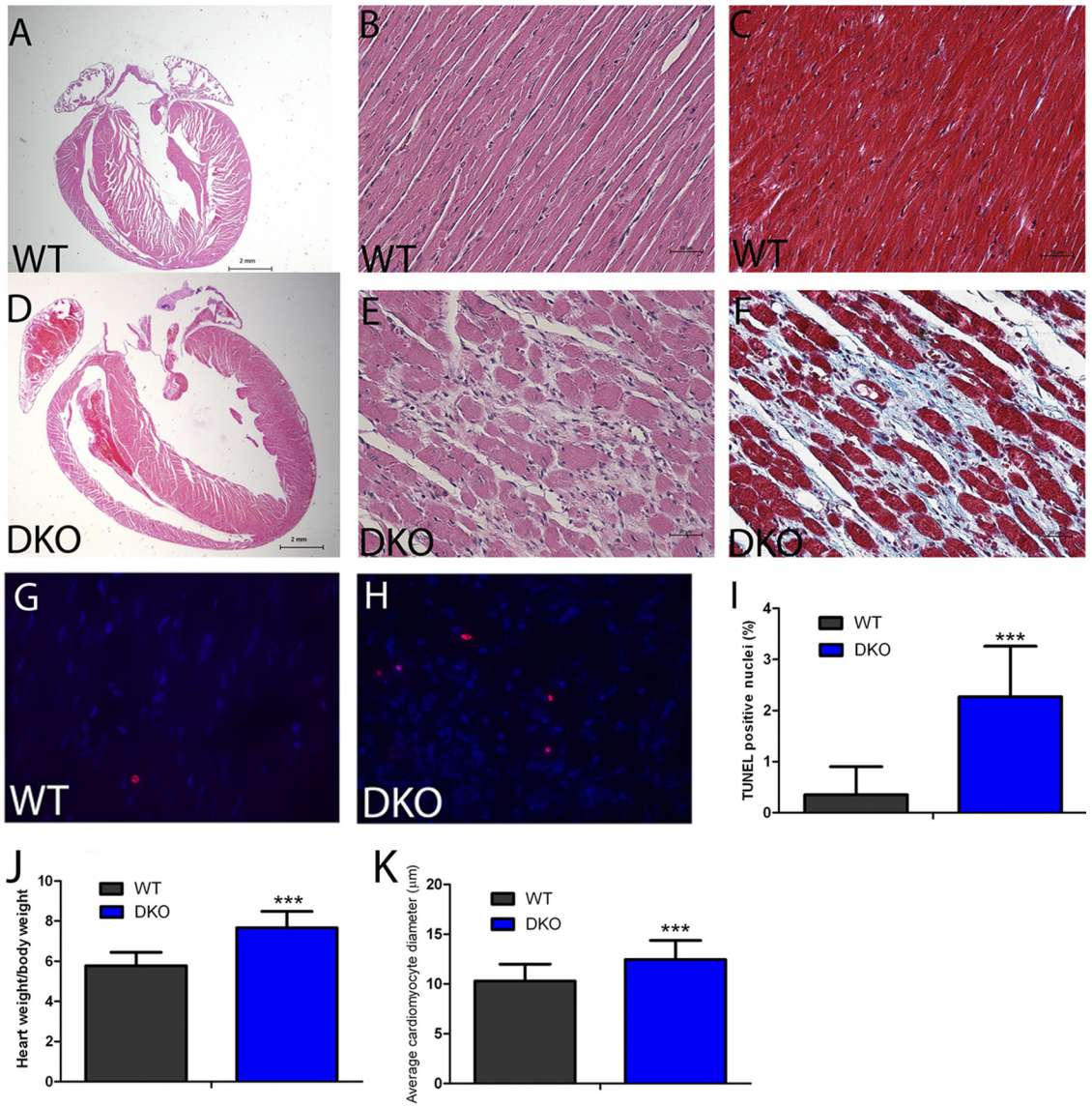

FIG 3 Histological analysis of PG/β-catenin DKO hearts. (A to F) Heart sections from PG$^{flox/flox}$/β-catenin$^{flox/flox}$; Cre^{-} (WT) and PG$^{flox/flox}$/β-catenin$^{flox/flox}$; Cre^{+} (DKO) mice 3 months after Tam administration were stained with H&E (A, B, D, and E) or Masson's trichrome (C and F). Note the extensive fibrosis in the DKO heart (F) compared with the WT heart (C). (G to I) TUNEL analysis of WT and DKO hearts ($n \geq 1{,}000$ nuclei from four different animals per group). (J) Quantification of heart weight/body weight ratios of WT and DKO mice at 3 months after Tam administration ($n = 30$ for each group). (K) Cardiomyocyte cross-sectional area quantification from histological sections of WT and DKO hearts at 3 months after Tam administration ($n \geq 100$ cells from at least five different animals per group). ***, $P < 0.001$.

ICD that is consistent with the severe cardiomyopathy observed in the DKO mice.

Loss of intercalated disc structures and impaired cardiac function in PG/β-catenin DKO mice. To examine myocyte junctions at the ultrastructural level, transmission electron microscopy was performed on DKO mouse hearts. ICD structures were readily visible in the WT hearts, with adherens junctions and desmosomes represented by submembranous electron-dense material adjacent to intercellular space between the myocytes (Fig. 6A). In contrast, normal ICD structures were absent in the DKO hearts, reminiscent of the N-cadherin CKO model (25). At higher magnification, the sarcomeres in DKO mouse hearts appeared distorted and compressed compared with the sarcomeres in WT mice (Fig. 6B and D), with decreased length (1,131.4 $\pm$ 68.7 nm versus 1,324.7 $\pm$ 41.23 nm for DKO versus WT mice, respectively, $P < 0.001$). The sarcomere defects in the DKO myocardium presumably reflect the lack of myofibril anchorage at the plasma membrane due to loss of the N-cadherin/catenin complex, resulting in decreased myofibril tension.

To assess cardiac function, M-mode two-dimensional echocardiography was performed on DKO mice 3 months after Tam administration. Quantitative image analysis demonstrated increased left ventricular (LV) end-systolic and -diastolic internal dimension (LVID) and volume in DKO hearts compared to these measures in WT hearts (Fig. 6E and F). Both LV ejection fraction (EF) and fractional shortening (FS) were reduced in DKO mice.

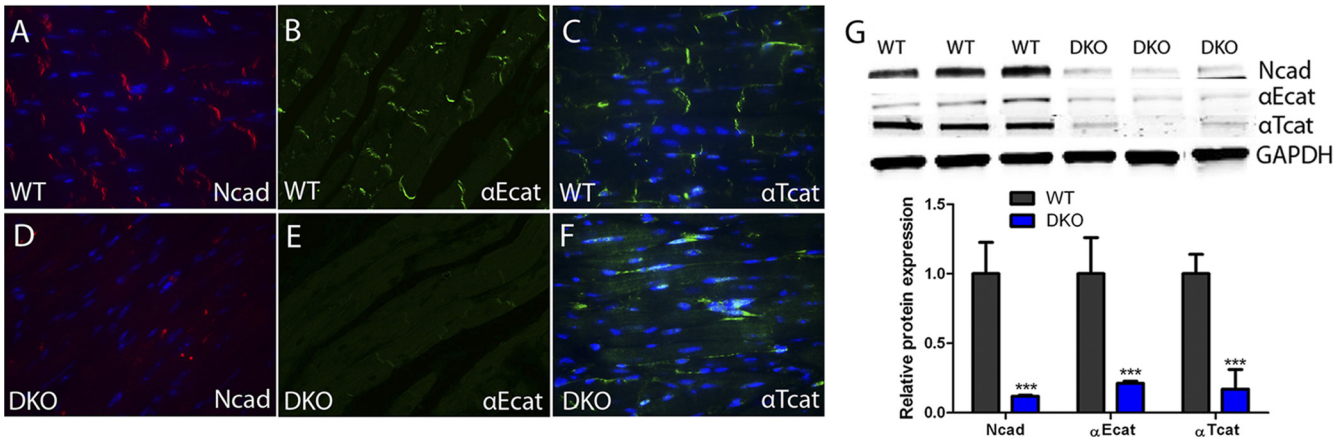

FIG 4 ICD expression of adherens junctional proteins in PG/β-catenin DKO hearts. (A to F) Heart sections from $PG^{flox/flox}$/β-$catenin^{flox/flox}$; Cre^{-} (WT) (A to C) and $PG^{flox/flox}$/β-$catenin^{flox/flox}$; Cre^{+} (DKO) (D to F) mice at 3 months after administration of Tam were immunostained for N-cadherin (Ncad) (A and D), αE-catenin (αEcat) (B and E), and αT-catenin (αTcat) (C and F). (G) Heart lysates from WT and DKO mice were immunoblotted for N-cadherin, αE-catenin, and αT-catenin. Note the decreased expression of each adherens junctional component in the DKO hearts compared with the levels in WT hearts ($n = 8$, WT; $n = 10$, DKO). ***, $P < 0.001$.

LV posterior (LVPW) and anterior (LVAW) wall thickness were increased in DKO mice, further validating cardiac hypertrophy at both the organ and cellular level (Fig. 3G and H). Doppler interrogation of DKO hearts revealed diminished flow velocities of both the pulmonary (PV) and aortic valves (AoV) (Fig. 6).

PG/β-catenin DKO mice exhibit conduction abnormalities. The fully penetrant sudden-death phenotype suggested that the DKO mice suffer from cardiac conduction abnormalities. Electrophysiological analysis using volumetric ECG recordings indicated longer PR intervals (44.3 ± 0.9 ms [$n = 9$, DKO mice] versus 38.8 ± 1.0 ms [$n = 9$, WT mice], $P < 0.01$) and increased QRS complex width (15.2 ± 0.4 ms [$n = 9$, DKO mice] versus 12.4 ± 0.4 ms [$n = 9$, WT mice], $P < 0.01$), consistent with a high propensity for arrhythmias (Fig. 7A). To determine susceptibility to induced arrhythmias, ventricular programmed electrical stimulation was performed on the DKO hearts 3 months after Tam administration as previously described for the PG CKO model (31). Burst ventricular pacing at a cycle length of 50 ms induced ventricular fibrillation in DKO hearts (8/11), resulting in cardiac arrest, whereas WT hearts (0/9) were able to regain normal sinus rhythm following stimulation (Fig. 7B). To monitor heart rhythms in conscious mice, miniaturized telemetric monitors were implanted in DKO mice about 3 months after Tam administration. We successfully captured ventricular arrhythmias in DKO animals (2/3), coincident with sudden death (Fig. 7C). Thus, unlike PG CKO animals that are resistant to ventricular arrhythmias (31), the abrupt onset of spontaneous ventricular arrhythmias in the DKO animals suggests disruption of gap junction communication between the DKO cardiomyocytes.

Gap junction remodeling in single CKO and PG/β-catenin DKO mice. Previous studies from our laboratory have shown that N-cadherin is critical for maintaining large Cx43-containing gap junction plaques at the ICD (28, 29). A recent study has shown that ischemic stress severs the interaction between the N-cad-

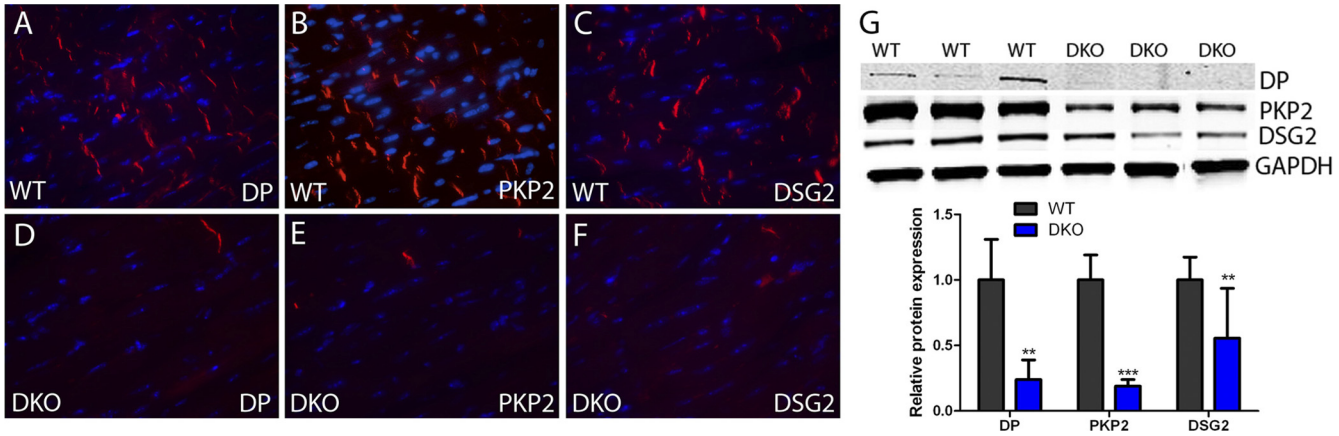

FIG 5 ICD expression of desmosomal proteins in PG/β-catenin DKO hearts. (A to F) Heart sections from $PG^{flox/flox}$/β-$catenin^{flox/flox}$; Cre^{-} (WT) (A to C) and $PG^{flox/flox}$/β-$catenin^{flox/flox}$; Cre^{+} (DKO) (D to F) mice at 3 months after administration of Tam were immunostained for desmoplakin (DP) (A and D), plakophilin-2 (PKP2) (B and E), and desmoglein-2 (DSG2) (C and F). (G) Heart lysates from WT and DKO mice were immunoblotted for desmoplakin, plakophilin-2, and desmoglein-2. Note the decreased expression of each desmosomal component in the DKO compared with the WT hearts ($n = 8$, WT; $n = 10$, DKO). **, $P < 0.01$; ***, $P < 0.001$.

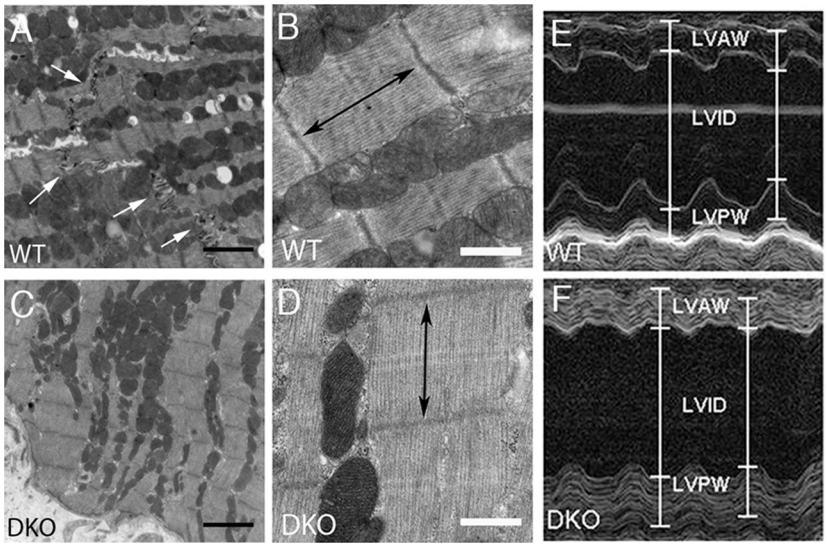

Echocardiographic indices of cardiac size and function

	WT	DKO	p
n	13	14	N/A
Gender (M/F)	9/4	8/6	N/A
Age (mo)	5	5	N/A
Post Tam (mo)	3	3	N/A
Body weight (g)	28.15 ± 3.91	28.04 ± 3.98	NS
Heart rate (bpm)	419.15 ± 40.1	438.21 ± 31.9	NS
LVID;s (mm)	2.34 ± 0.23	3.08 ± 0.34	p< 0.001
LVID;d (mm)	3.15 ± 0.24	3.82 ± 0.34	p< 0.001
LV vol;s (mm)	23.47 ± 3.62	37.84 ± 7.33	p< 0.001
LV vol;d (mm)	52.01 ± 5.49	68.16 ± 9.74	p< 0.001
EF (%)	61.08 ± 3.78	44.63 ± 4.03	p< 0.001
FS (%)	32.19 ± 2.83	21.78 ± 2.30	p< 0.001
LVPW;s (mm)	0.99 ± 0.10	1.30 ± 0.28	p< 0.01
LVPW;d (mm)	0.87 ± 0.11	1.18 ± 0.25	p< 0.01
LVAW;s (mm)	0.95 ± 0.15	1.22 ± 0.11	p< 0.001
LVAW;d (mm)	0.74 ± 0.16	1.10 ± 0.14	p< 0.001
PV mean V (mm/s)	671.3 ± 69.8	469.99 ± 115.3	p< 0.001
AoV mean V (mm/s)	836.27 ± 109.4	611.64 ± 130.8	p< 0.01

FIG 6 Ultrastructural and echocardiographic analysis of PG/β-catenin DKO mice. (A to D) Transmission electron micrographs of LV myocardium from $PG^{flox/flox}$/β-$catenin^{flox/flox}$; Cre^{-} (WT) (A and B) and $PG^{flox/flox}$/β-$catenin^{flox/flox}$; Cre^{+} (DKO) (C and D) hearts at 3 months after administration of Tam ($n \geq$ 10 fields per heart from three different animals per group). Intercalated discs were readily visualized in the control hearts (A, arrows); in contrast, these structures were absent in the DKO hearts (C). DKO myocytes displayed decreased sarcomere length (double-headed arrow) (D). Bars indicate 2 μm (black) and 500 nm (white). (E and F) Representative M-mode two-dimensional echocardiography displaying LV chamber dilation in DKO compared to WT mice. Mean values of echocardiographic parameters are shown in the table. Data represent means ± standard deviations. Note significant increased LV end-systolic and -diastolic internal dimension (LVID) and volume (LV vol) and reduced LV ejection fraction (EF) and fraction shortening (FS) in DKO mice. N/A, not applicable; NS, not significant; M/F, male/female; bpm, beats per minute; V, velocity.

herin/catenin complex and Cx43, resulting in reduced Cx43 at the ICD, thus implicating N-cadherin directly in gap junction remodeling in diseased myocardium (46). To investigate whether altered gap junctions correlate with the arrhythmogenic phenotype in the DKO mice, we compared Cx43 expression in the single-CKO and DKO mice. Initially, coimmunoprecipitation was performed with anti-N-cadherin antibody and probed for β-catenin and PG to confirm the composition of the N-cadherin/catenin complex in the different genotypes (Fig. 8K). As predicted, PG association with N-cadherin was enhanced in the absence of β-catenin and vice versa, consistent with their increased expression at the ICD in the mutant hearts (31, 49). Importantly, the N-cadherin/catenin complex was remarkably decreased in the DKO hearts (Fig. 8K), consistent with depletion of both catenins and the overall decrease in N-cadherin levels (Fig. 4). Next, we examined the expression and distribution of gap junction protein Cx43 *in situ* (Fig. 8A to D), as well as in isolated cardiomyocytes (Fig. 8E to H) derived from the single-CKO and DKO hearts. The Cx43 immunostaining patterns were similar between the heart sections and the isolated cardiomyocytes, and hence, we chose the latter to determine how the size and area fraction of Cx43-containing gap junctions varied between each mouse model. Interestingly, we observed a stepwise decrease in Cx43 expression between the different strains, with WT > β-catenin CKO > PG CKO > DKO and the DKO hearts exhibiting dramatic reduction of Cx43 at the ICD. When β-catenin CKO hearts were compared to WT hearts, we found no significant change in the average size of Cx43-containing junction plaques (≥5 pixels) (Fig. 8I); however, the area occupied by gap junction plaques at the ICD was significantly reduced (~24.5%, $P < 0.001$) (Fig. 8J). PG CKO myocytes exhibited a further reduction in both average size (~42.5%, $P < 0.01$) and area occupied by gap junction plaques (~50.0%, $P < 0.001$) compared to WT myocytes. Finally, DKO cardiomyocytes displayed a striking decrease in average size (~85.9%, $P < 0.001$) and area occupied by gap junction plaques (~85.0%, $P < 0.001$), consistent with conduction abnormalities and arrhythmic death in the DKO mice. Moreover, N-cadherin/Cx43 association was significantly reduced in DKO compared to single-CKO hearts (Fig. 8K). The diseased myocardium often exhibits an increase in hypophosphorylated Cx43, along with its redistribution away from the ICD toward the lateral edges of cardiomyocytes (4). To determine if hypophosphorylated Cx43 levels were increased in the mutant hearts, we performed immunoblot analysis with an antibody that recognizes particular dephosphorylated serine residues in the large carboxy terminus of Cx43 (34). DKO animals exhibited a significant increase in levels of dephosphorylated Cx43 compared to the levels in single-CKO and WT hearts (Fig. 8L). Taken together, comparison of single-CKO and DKO mice illustrates the extent of gap junction remodeling necessary to elicit arrhythmias in these murine models.

Gap junction remodeling precedes the onset of arrhythmias. To investigate the relationship between arrhythmias and cardiomyopathy, PG/β-catenin DKO hearts were examined at 3, 5, and 8 weeks after Tam administration to correlate changes in cardiac pathology, function, and arrhythmia susceptibility. Interestingly, as early as 3 weeks after Tam administration, DKO mice exhibited signs of cardiac dysfunction (Fig. 9M and N) and aberrant pathology, including fibrosis (Fig. 9B). The early onset of the phenotype correlated with decreased N-cadherin at the ICD (Fig. 9F). Furthermore, gap junction remodeling was also observed at this early time point before the onset of inducible arrhythmias (Fig. 9J and O). Taken together, these data indicate that cardiomyopathy and gap junction remodeling occur prior to arrhythmia susceptibility in the DKO mouse model, suggesting that additional molecular

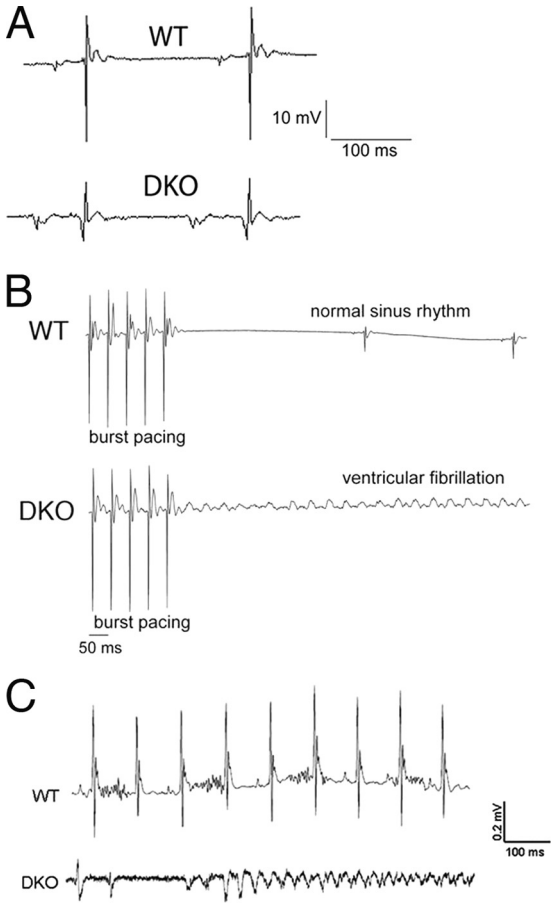

FIG 7 Inducible and spontaneous ventricular arrhythmias recorded in PG/β-catenin DKO hearts. (A) Representative volume-conducted ECG recordings prior to burst pacing. Note the global low voltage signal in the DKO hearts prior to stimulation. Measurements of ECG recordings revealed increased PR and QRS intervals. (B) Following burst pacing, ventricular fibrillation was only observed in the DKO group (8/11) and not in WT mice (0/9) ($P < 0.01$). (C) Representative telemetric ECG recordings from a miniaturized transmitter implanted in awake, freely mobile animals captured lethal ventricular arrhythmias in DKO mice (2/3), whereas WT mice showed normal sinus rhythm.

and/or structural changes are necessary for the arrhythmogenic substrate.

DISCUSSION

The identification of mutations in genes encoding desmosomal proteins in arrhythmogenic right ventricular cardiomyopathy (ARVC) has highlighted the importance of proper mechanical coupling in the regulation of gap junction organization in human disease (7, 14, 15, 40, 42). It is now recognized that this disease often affects both left and right ventricles, and hence, a broader term of arrhythmic cardiomyopathy is now considered appropriate for this disease (42). Studies of individuals from the Greek island of Naxos identified an autosomal recessive form of ARVC with palmoplantar keratoderma and woolly hair referred to as Naxos disease (36). Gene sequencing revealed a homozygous 2-bp deletion (2157-2158delGT) in the *plakoglobin* (*JUP*) gene as the genetic cause of Naxos disease (32). A dominantly inherited *PG* gene mutation (S39_K40insS) was recently identified in ARVC patients without cutaneous abnormalities (5). Both mutant forms of PG fail to localize properly at the ICD, and the junctional components desmoplakin and Cx43 are significantly reduced at the ICD in these patients. Ultrastructural investigation showed ICD remodeling with mislocalization and decreased numbers of desmosomes (5, 8). We recently deleted the PG gene specifically in the myocardium in order to generate an animal model of ARVC without the cutaneous syndrome (31). The PG cardiac-specific conditional knockout (CKO) recapitulates many of the pathological features of ARVC, including myocyte loss, replacement fibrosis, inflammation, and dilated cardiomyopathy. However, despite gap junction remodeling, we did not observe conduction abnormalities or increased susceptibility to arrhythmias in the PG CKO mice. The inability to induce arrhythmias was unexpected as it was reported that PG heterozygous null animals are susceptible to induced ventricular arrhythmias with no apparent change in Cx43 expression (24). In contrast to the PG CKO model, β-catenin expression is not increased in the $PG^{-/+}$ hearts that exhibit arrhythmias (16), suggesting that the increased β-catenin may be protecting the PG CKO mice from arrhythmias. Recently, β-catenin was reported to be upregulated in a noninducible cardiac tissue-specific PG knockout model (27). In this murine model, deletion of the PG gene during the perinatal and postnatal period with the αMHC/Cre transgene (2) results in rapid development of the ARVC phenotype in these animals. Depletion of PG in the early postnatal heart likely explains the more severe pathology observed in these animals compared to that in our inducible PG CKO model (31) in which PG is depleted from the adult heart. The extensive cardiac remodeling in the noninducible αMHC/Cre; $PG^{flox/flox}$ mice may explain, at least in part, the increased arrhythmogenicity in that model compared to that in the inducible PG CKO model. Future studies will be necessary to address this possibility.

The present study was performed to explore the significance of increased β-catenin expression at the ICD and its potential role in regulating gap junction organization and arrhythmogenicity in the PG CKO mice. To address this possibility, we performed immunoprecipitation experiments and found an increased association between Cx43 and β-catenin in the absence of PG. Despite this increased interaction, gap junction plaques were significantly smaller in the PG CKO than in the β-catenin CKO and wild-type cardiomyocytes. In Naxos disease (23), as well as experimental models of ischemia (46), N-cadherin levels at the ICD remain unchanged. However, it is the association of N-cadherin with Cx43 that is critically important for proper gap junction organization at the ICD and electrical coupling between cardiomyocytes (46). In this regard, it is important to emphasize that N-cadherin association with Cx43, as determined by immunoprecipitation, did not change in PG CKO heart lysates compared to the level of association in wild-type heart lysates. In contrast, N-cadherin/Cx43 association is reduced in the DKO hearts, consistent with the dramatic gap junction remodeling and SCD. We conclude from the results of these experiments that, although reduced, the remaining gap junctions in PG CKO hearts are sufficient to maintain proper electrical conduction, at least under nonstressed conditions.

A decrease in β-catenin and Cx43 has been noted in animal models of cardiomyopathy, suggesting that β-catenin may play a causal role in gap junction remodeling and subsequent arrhythmogenesis in those models (3, 48). Conversely, inhibiting GSK3β with lithium stabilizes β-catenin and increases its association with

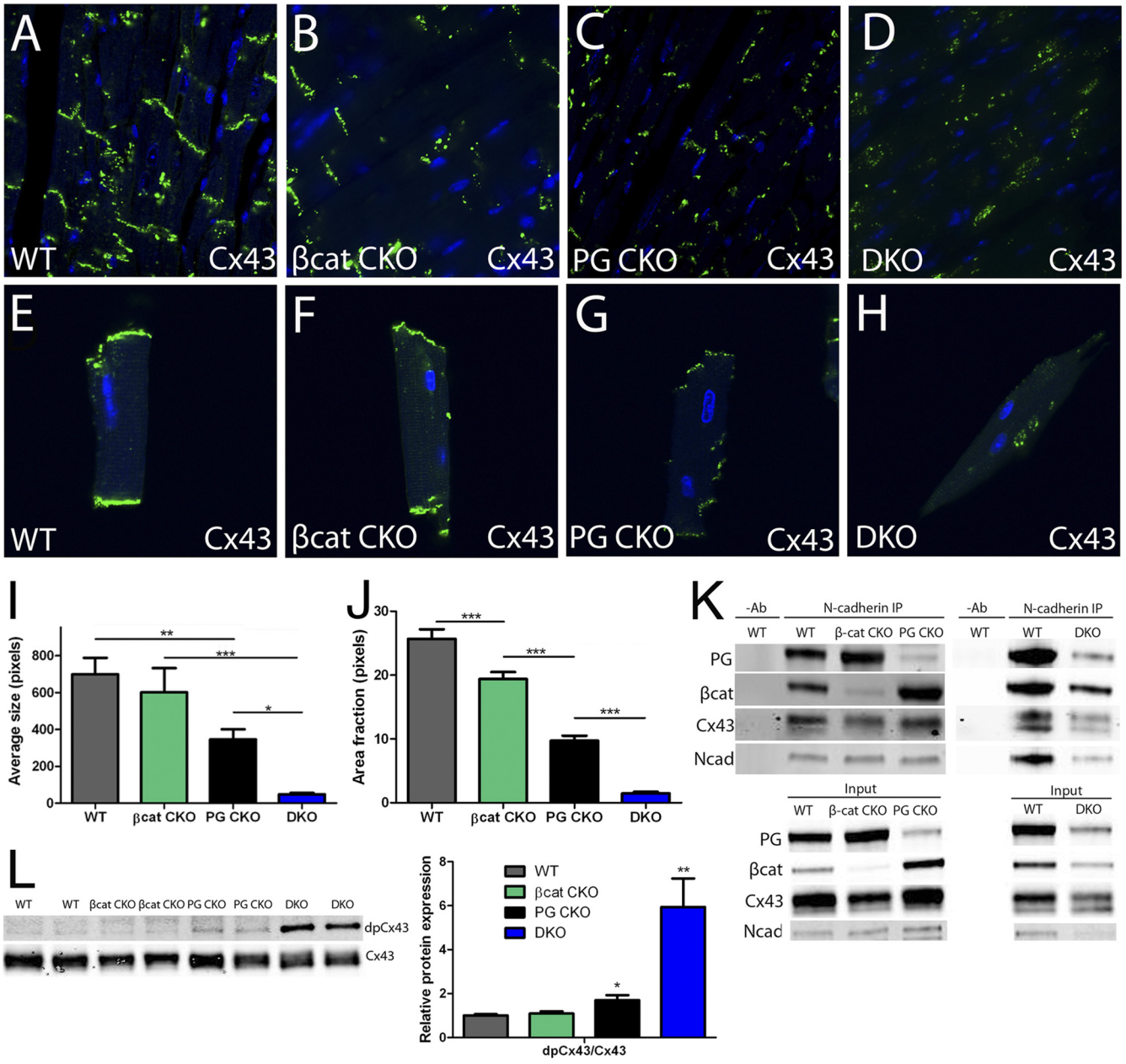

FIG 8 Cx43 expression and protein interactions in single-CKO and DKO hearts. (A to D) Heart sections from $PG^{flox/flox}$/β-$catenin^{flox/flox}$; Cre^{-} (WT) (A), β-$catenin^{flox/flox}$; Cre^{+} (βcat CKO) (B), $PG^{flox/flox}$; Cre^{+} (PG CKO) (C), and $PG^{flox/flox}$/β-$catenin^{flox/flox}$; Cre^{+} (DKO) (D) mice were immunostained for Cx43 3 months after Tam administration. (E to H) Representative images of isolated cardiomyocytes from WT (E), β-catenin CKO (F), PG CKO (G), and DKO (H) hearts immunostained for Cx43. Quantitative immunofluorescence microscopy was performed on 20 test areas (ICD regions). (I, J) The average size (I) and area fraction (J) occupied by Cx43-containing clusters for each genotype are shown. (K) Heart lysates were immunoprecipitated with anti-N-cadherin antibody and subsequently immunoblotted for PG, β-catenin (βcat), Cx43, and N-cadherin (Ncad). No-antibody IP served as the negative control (−Ab). Note the significant decrease of the N-cadherin/catenin/Cx43 macromolecular complex in the DKO hearts, whereas the single-CKO hearts maintain the multiprotein complex. (L) Heart lysates from WT, β-catenin CKO, PG CKO, and DKO mice were immunoblotted for dephosphorylated Cx43 (dpCx43) and total Cx43. Note the significant increase in dpCx43 in DKO hearts. *, $P < 0.05$; **, $P < 0.01$; ***, $P < 0.001$.

Cx43, resulting in increased dye coupling between rat cardiomyocytes (3). Importantly, β-catenin has been shown to be essential for microtubule-mediated connexon trafficking to the plasma membrane in HeLa cells (44). It should be noted that possible effects of PG on gap junction remodeling were not considered in the above-described studies. Of relevance to our studies, it was reported that depletion of β-catenin in the adult myocardium using inducible αMHC/MerCreMer (49) or MLC2v/Cre (22) did not result in cardiomyopathy, and importantly, Cx43 expression appeared normal in the β-catenin-deficient myocardium. In the present study, we also did not observe cardiomyopathy in the αMHC/MerCreMer; β-catenin floxed mice after Tam administration; however, we did observe a modest reduction in Cx43 expression in the absence of β-catenin. This apparent discrepancy is

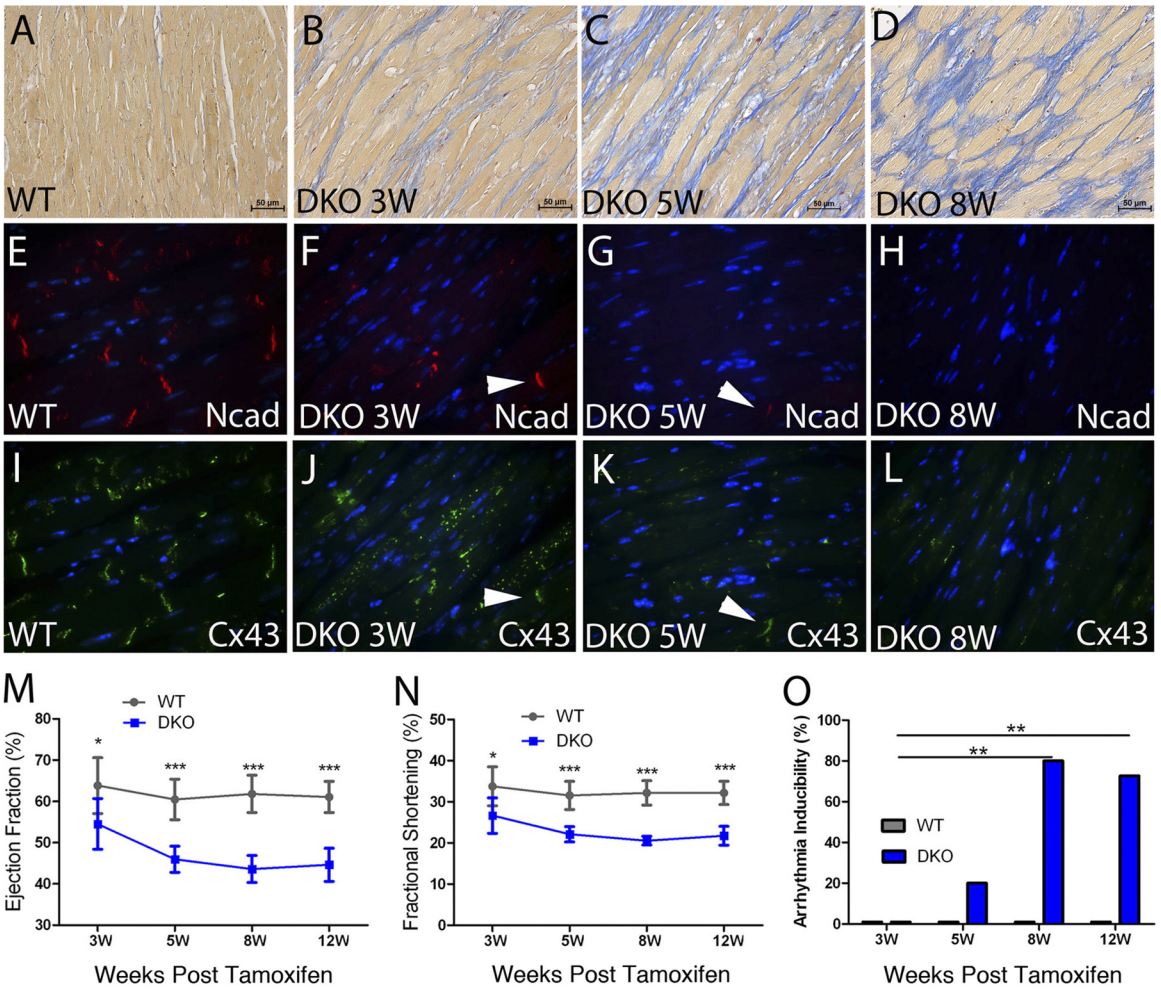

FIG 9 Relationship between cardiomyopathy, gap junction remodeling, and arrhythmic susceptibility in the DKO mice. (A to D) Heart sections from $PG^{flox/flox}/\beta\text{-catenin}^{flox/flox}$; Cre^{-} (WT) and $PG^{flox/flox}/\beta\text{-catenin}^{flox/flox}$; Cre^{+} (DKO) mice were stained with acid fuchsin orange G at 3 (3W) (B), 5 (5W) (C), and 8 (8W) (D) weeks after Tam administration. Note the fibrotic response as early as 3 weeks in DKO hearts (B) compared with WT hearts (A). (E to L) Heart sections were immunostained for N-cadherin (Ncad, red) and connexin43 (Cx43, green) at 3 (F, J), 5 (G and K), and 8 (H and L) weeks, respectively, after Tam administration. Note the decreased localization of both Ncad and Cx43 at the intercalated disc (ID) as early as 3 weeks after Tam administration. Arrowheads denote remaining N-cadherin/Cx43 colocalization at the ID. Ejection fraction (M) and fractional shortening (N) of DKO and WT hearts at 3, 5, 8, and 12 weeks after Tam administration as determined by echocardiography. The incidence of ventricular fibrillation in DKO hearts following burst pacing protocol was not significantly different at 3 (0/4) or 5 (1/5) weeks after Tam administration compared to that in the WT (0/10). However, the percentage of DKO hearts susceptible to induced arrhythmia at 8 (4/5) and 12 (8/11) weeks after Tam administration differed compared to the results for DKO mice at 3 weeks after Tam administration. *, $P < 0.05$; **, $P < 0.01$; ***, $P < 0.001$.

probably due to the detailed characterization of Cx43 expression performed in our study (i.e., quantitative confocal microscopy) in comparison to the analysis in previous studies (22, 49). Taken together, β-catenin probably plays a role in trafficking of Cx43 to the ICD; however, the upregulation of PG functionally compensates for loss of β-catenin, resulting in normal cardiac histology (49) with a modest reduction of Cx43 at the ICD (this study).

We previously reported a decrease in the number of cardiac desmosomes in PG CKO mice, resulting in progressive cardiomyopathy despite upregulation of β-catenin at the ICD (31). In PG-null keratinocytes, β-catenin is capable of binding the cytoplasmic domain of desmosomal cadherins; however, it is unable to provide a functional linkage via desmoplakin, leading to altered desmosome organization (1, 10). Together, these findings emphasize the importance of PG in maintaining normal desmosome structure and that β-catenin is not able to functionally substitute for PG in linking desmosomal cadherins to intermediate filaments. Interestingly, recent data indicate that mixing of adherens junctional and desmosomal components at the ICD results in a novel hybrid adhering junction or area composita (11, 17, 19). Hence, loss of PG in the heart will affect both the desmosome proper and the desmosomal junctions found in the area composita. β-Catenin has been shown to be important for microtubule-mediated connexon trafficking to the plasma membrane (44), and β-catenin is increased at the ICD in the absence of PG; hence, we speculate that gap junction remodeling in the PG CKO is probably due to the disruption of desmosome function and not the inability to tether microtubules to the ICD via the N-cadherin/β-catenin complex. Future experiments will be necessary to address this and alternative possibilities. It should be noted that the role of PG in con-

nexon trafficking, assembly, and stabilization at the membrane has not been previously studied. Importantly, we readily identified PG in the Cx43 immunoprecipitate in the wild-type hearts, consistent with the idea that these two closely related armadillo proteins are functionally interchangeable in the N-cadherin/catenin/Cx43 macromolecular complex. Taken together, we conclude that β-catenin and PG are interchangeable for N-cadherin-mediated trafficking of connexons to the plasma membrane; however, additional studies are required to show direct interaction between PG and gap junction trafficking machinery.

We have previously shown that N-cadherin is required for maintaining ICD structure and that loss of N-cadherin results in gap junction remodeling and spontaneous lethal ventricular arrhythmias (25, 29). The DKO model has many similarities to the N-cadherin CKO model, including disassembly of the ICD, gap junction remodeling, and SCD in 100% of the animals. An interesting difference between the models is the lack of myocyte cell death and replacement fibrosis seen in the N-cadherin CKO hearts compared to either the PG CKO (31) or the PG/β-catenin DKO animals (this study). Based on the cardiac phenotypes of the various junctional protein knockout models (18, 25, 31, 45), we conclude that there are distinct signaling pathways downstream from the two mechanical junction complexes. If the primary defect occurs in a desmosomal component, the phenotype resembles ARVC pathology, with loss of myocytes, inflammation, and replacement fibrosis, whereas loss of N-cadherin alone produces cardiomyopathy accompanied by an interstitial fibrosis response.

Compared to the PG CKO hearts, there was dramatic gap junction remodeling in the DKO hearts, consistent with the loss of the N-cadherin/catenin complex at the ICD. The phosphorylation status of several serine residues within the large carboxy-terminal tail of Cx43 is associated with the formation of active gap junction channels at the cell surface. In contrast, the same residues are generally dephosphorylated during trafficking/endocytosis in the cytoplasm. This phenomenon is also observed in diseased myocardium, consistent with electrical uncoupling and increased susceptibility to arrhythmias (4). In a seminal study, Cx43 knock-in alleles were generated consisting of either three serine residues replaced by nonphosphorylatable alanines (S3A) or phosphomimetic glutamic acids (S3E) to directly determine the requirement for phosphorylated Cx43 in proper electrical coupling in the heart (37). The authors showed that the S3A mice are susceptible to induced arrhythmias whereas the S3E mice are resistant to arrhythmias, demonstrating the importance of Cx43 phosphorylation for proper electrical coupling *in vivo*. We previously observed increased dephosphorylated Cx43, albeit at different serine residues, along with increased susceptibility to arrhythmias in the N-cadherin CKO (29) and N-cadherin heterozygous null animals (28). In this study, DKO hearts exhibited a significant increase in dephosphorylated Cx43, consistent with less functional gap junctions and spontaneous lethal arrhythmias in the DKO mice. In addition to gap junction remodeling, ion channel remodeling probably contributes to the arrhythmogenic substrate in the DKO mice, as we recently reported aberrant Kv1.5 channel function in the N-cadherin CKO model (13). Collectively, the arrhythmogenic phenotype in the DKO mice reinforces the importance of the N-cadherin/catenin complex in the establishment and maintenance of gap junctions at the ICD.

In conclusion, our study provides the first *in vivo* evidence that PG and β-catenin are required to anchor the N-cadherin/catenin adhesion complex to the cytoskeleton and that loss of this linkage leads to disassembly of the cardiac ICD structure and lethal arrhythmias. In future studies, comparison of Cx43-containing plaques in the single and double mutant mice will allow further assessment of the relative contributions of PG and β-catenin in connexon trafficking, assembly, and stabilization at the ICD, which may have implications for understanding arrhythmogenesis observed in ARVC patients.

ACKNOWLEDGMENTS

We thank Leeanne Griffith, Andrew Ho, and Jonathan Gordon for technical assistance.

We thank the Bioimaging Facility of the Kimmel Cancer Center (NIH Cancer Center Core grant 5 P30 CA-56036) for use of the confocal microscope. This work was supported by the National Institutes of Health (grants HL081569 to G.L.R. and T32AR052273 to D.S.) and an American Heart Association predoctoral fellowship (PRE7360047 to D.S.) and American Heart Association Scientist Development grant (N2080068 to J.L.).

REFERENCES

1. **Acehan D, et al.** 2008. Plakoglobin is required for effective intermediate filament anchorage to desmosomes. J. Invest. Dermatol. **128**:2665–2675.
2. **Agah R, et al.** 1997. Gene recombination in postmitotic cells. Targeted expression of Cre recombinase provokes cardiac-restricted, site-specific rearrangement in adult ventricular muscle in vivo. J. Clin. Invest. **100**: 169–179.
3. **Ai Z, Fischer A, Spray DC, Brown AM, Fishman GI.** 2000. Wnt-1 regulation of connexin43 in cardiac myocytes. J. Clin. Invest. **105**:161–171.
4. **Akar FG, Spragg DD, Tunin RS, Kass DA, Tomaselli GF.** 2004. Mechanisms underlying conduction slowing and arrhythmogenesis in nonischemic dilated cardiomyopathy. Circ. Res. **95**:717–725.
5. **Asimaki A, et al.** 2007. A novel dominant mutation in plakoglobin causes arrhythmogenic right ventricular cardiomyopathy. Am. J. Hum. Genet. **81**:964–973.
6. **Asimaki A, et al.** 2009. A new diagnostic test for arrhythmogenic right ventricular cardiomyopathy. N. Engl. J. Med. **360**:1075–1084.
7. **Basso C, Corrado D, Marcus FI, Nava A, Thiene G.** 2009. Arrhythmogenic right ventricular cardiomyopathy. Lancet **373**:1289–1300.
8. **Basso C, et al.** 2006. Ultrastructural evidence of intercalated disc remodelling in arrhythmogenic right ventricular cardiomyopathy: an electron microscopy investigation on endomyocardial biopsies. Eur. Heart J. **27**: 1847–1854.
9. **Bierkamp C, McLaughlin KJ, Schwarz H, Huber O, Kemler R.** 1996. Embryonic heart and skin defects in mice lacking plakoglobin. Dev. Biol. **180**:780–785.
10. **Bierkamp C, Schwarz H, Huber O, Kemler R.** 1999. Desmosomal localization of beta-catenin in the skin of plakoglobin null-mutant mice. Development **126**:371–381.
11. **Borrmann CM, et al.** 2006. The area composita of adhering junctions connecting heart muscle cells of vertebrates. II. Colocalizations of desmosomal and fascia adhaerens molecules in the intercalated disk. Eur. J. Cell Biol. **85**:469–485.
12. **Chen X, et al.** 2006. The beta-catenin/T-cell factor/lymphocyte enhancer factor signaling pathway is required for normal and stress-induced cardiac hypertrophy. Mol. Cell. Biol. **26**:4462–4473.
13. **Cheng L, Yung A, Covarrubias M, Radice GL.** 2011. Cortactin is required for N-cadherin regulation of Kv1.5 channel function. J. Biol. Chem. **286**:20478–20489.
14. **Delmar M, McKenna WJ.** 2010. The cardiac desmosome and arrhythmogenic cardiomyopathies: from gene to disease. Circ. Res. **107**:700–714.
15. **den Haan AD, et al.** 2009. Comprehensive desmosome mutation analysis in North Americans with arrhythmogenic right ventricular dysplasia/cardiomyopathy. Circ. Cardiovasc. Genet. **2**:428–435.
16. **Fabritz L, et al.** 2011. Load-reducing therapy prevents development of arrhythmogenic right ventricular cardiomyopathy in plakoglobin-deficient mice. J. Am. Coll. Cardiol. **57**:740–750.
17. **Franke WW, Borrmann CM, Grund C, Pieperhoff S.** 2006. The area

composita of adhering junctions connecting heart muscle cells of vertebrates. I. Molecular definition in intercalated disks of cardiomyocytes by immunoelectron microscopy of desmosomal proteins. Eur. J. Cell Biol. **85**:69–82.
18. **Garcia-Gras E, et al.** 2006. Suppression of canonical Wnt/beta-catenin signaling by nuclear plakoglobin recapitulates phenotype of arrhythmogenic right ventricular cardiomyopathy. J. Clin. Invest. **116**:2012–2021.
19. **Goossens S, et al.** 2007. A unique and specific interaction between alphaT-catenin and plakophilin-2 in the area composita, the mixed-type junctional structure of cardiac intercalated discs. J. Cell Sci. **120**:2126–2136.
20. **Green KJ, Simpson CL.** 2007. Desmosomes: new perspectives on a classic. J. Invest. Dermatol. **127**:2499–2515.
21. **Gutstein DE, et al.** 2001. Conduction slowing and sudden arrhythmic death in mice with cardiac-restricted inactivation of connexin43. Circ. Res. **88**:333–339.
22. **Hirschy A, et al.** 2010. Stabilised beta-catenin in postnatal ventricular myocardium leads to dilated cardiomyopathy and premature death. Basic Res. Cardiol. **105**:597–608.
23. **Kaplan SR, et al.** 2004. Remodeling of myocyte gap junctions in arrhythmogenic right ventricular cardiomyopathy due to a deletion in plakoglobin (Naxos disease). Heart Rhythm **1**:3–11.
24. **Kirchhof P, et al.** 2006. Age- and training-dependent development of arrhythmogenic right ventricular cardiomyopathy in heterozygous plakoglobin-deficient mice. Circulation **114**:1799–1806.
25. **Kostetskii I, et al.** 2005. Induced deletion of the N-cadherin gene in the heart leads to dissolution of the intercalated disc structure. Circ. Res. **96**:346–354.
26. **Kramer K, et al.** 1993. Use of telemetry to record electrocardiogram and heart rate in freely moving mice. J. Pharmacol. Toxicol. Methods **30**:209–215.
27. **Li D, et al.** 2011. Restrictive loss of plakoglobin in cardiomyocytes leads to arrhythmogenic cardiomyopathy. Hum. Mol. Genet. **20**:4582–4596.
28. **Li J, et al.** 2008. N-cadherin haploinsufficiency affects cardiac gap junctions and arrhythmic susceptibility. J. Mol. Cell. Cardiol. **44**:597–606.
29. **Li J, et al.** 2005. Cardiac-specific loss of N-cadherin leads to alteration in connexins with conduction slowing and arrhythmogenesis. Circ. Res. **97**:474–481.
30. **Li J, Patel VV, Radice GL.** 2006. Dysregulation of cell adhesion proteins and cardiac arrhythmogenesis. Clin. Med. Res. **4**:42–52.
31. **Li J, et al.** 2011. Cardiac tissue-restricted deletion of plakoglobin results in progressive cardiomyopathy and activation of β-catenin signaling. Mol. Cell. Biol. **31**:1134–1144.
32. **McKoy G, et al.** 2000. Identification of a deletion in plakoglobin in arrhythmogenic right ventricular cardiomyopathy with palmoplantar keratoderma and woolly hair (Naxos disease). Lancet **355**:2119–2124.
33. **Mitra R, Morad M.** 1985. A uniform enzymatic method for dissociation of myocytes from hearts and stomachs of vertebrates. Am. J. Physiol. **249**:H1056–H1060.
34. **Nagy JI, et al.** 1997. Selective monoclonal antibody recognition and cellular localization of an unphosphorylated form of connexin43. Exp. Cell Res. **236**:127–136.
35. **Peters NS, Green CR, Poole-Wilson PA, Severs NJ.** 1993. Reduced content of connexin43 gap junctions in ventricular myocardium from hypertrophied and ischemic human hearts. Circulation **88**:864–875.
36. **Protonotarios N, et al.** 1986. Cardiac abnormalities in familial palmoplantar keratosis. Br. Heart J. **56**:321–326.
37. **Remo BF, et al.** 2011. Phosphatase-resistant gap junctions inhibit pathological remodeling and prevent arrhythmias. Circ. Res. **108**:1459–1466.
38. **Ruiz P, et al.** 1996. Targeted mutation of plakoglobin in mice reveals essential functions of desmosomes in the embryonic heart. J. Cell Biol. **135**:215–225.
39. **Saffitz JE.** 2006. Adhesion molecules: why they are important to the electrophysiologist. J. Cardiovasc. Electrophysiol. **17**:225–229.
40. **Saffitz JE.** 2009. Arrhythmogenic cardiomyopathy and abnormalities of cell-to-cell coupling. Heart Rhythm **6**:S62–S65.
41. **Saffitz JE, Green KG, Kraft WJ, Schechtman KB, Yamada KA.** 2000. Effects of diminished expression of connexin43 on gap junction number and size in ventricular myocardium. Am. J. Physiol. Heart Circ. Physiol. **278**:H1662–H1670.
42. **Sen-Chowdhry S, Morgan RD, Chambers JC, McKenna WJ.** 2010. Arrhythmogenic cardiomyopathy: etiology, diagnosis, and treatment. Annu. Rev. Med. **61**:233–253.
43. **Shapiro L, et al.** 1995. Structural basis of cell-cell adhesion by cadherins. Nature **374**:327–337.
44. **Shaw RM, et al.** 2007. Microtubule plus-end-tracking proteins target gap junctions directly from the cell interior to adherens junctions. Cell **128**:547–560.
45. **Sheikh F, et al.** 2006. alpha-E-catenin inactivation disrupts the cardiomyocyte adherens junction, resulting in cardiomyopathy and susceptibility to wall rupture. Circulation **114**:1046–1055.
46. **Smyth JW, et al.** 2010. Limited forward trafficking of connexin 43 reduces cell-cell coupling in stressed human and mouse myocardium. J. Clin. Invest. **120**:266–279.
47. **Sohal DS, et al.** 2001. Temporally regulated and tissue-specific gene manipulations in the adult and embryonic heart using a tamoxifen-inducible Cre protein. Circ. Res. **89**:20–25.
48. **Yoshida M, et al.** 2011. Alterations in adhesion junction precede gap junction remodelling during the development of heart failure in cardiomyopathic hamsters. Cardiovasc. Res. **92**:95–105.
49. **Zhou J, et al.** 2007. Upregulation of gamma-catenin compensates for the loss of beta-catenin in adult cardiomyocytes. Am. J. Physiol. Heart Circ. Physiol. **292**:H270–H276.